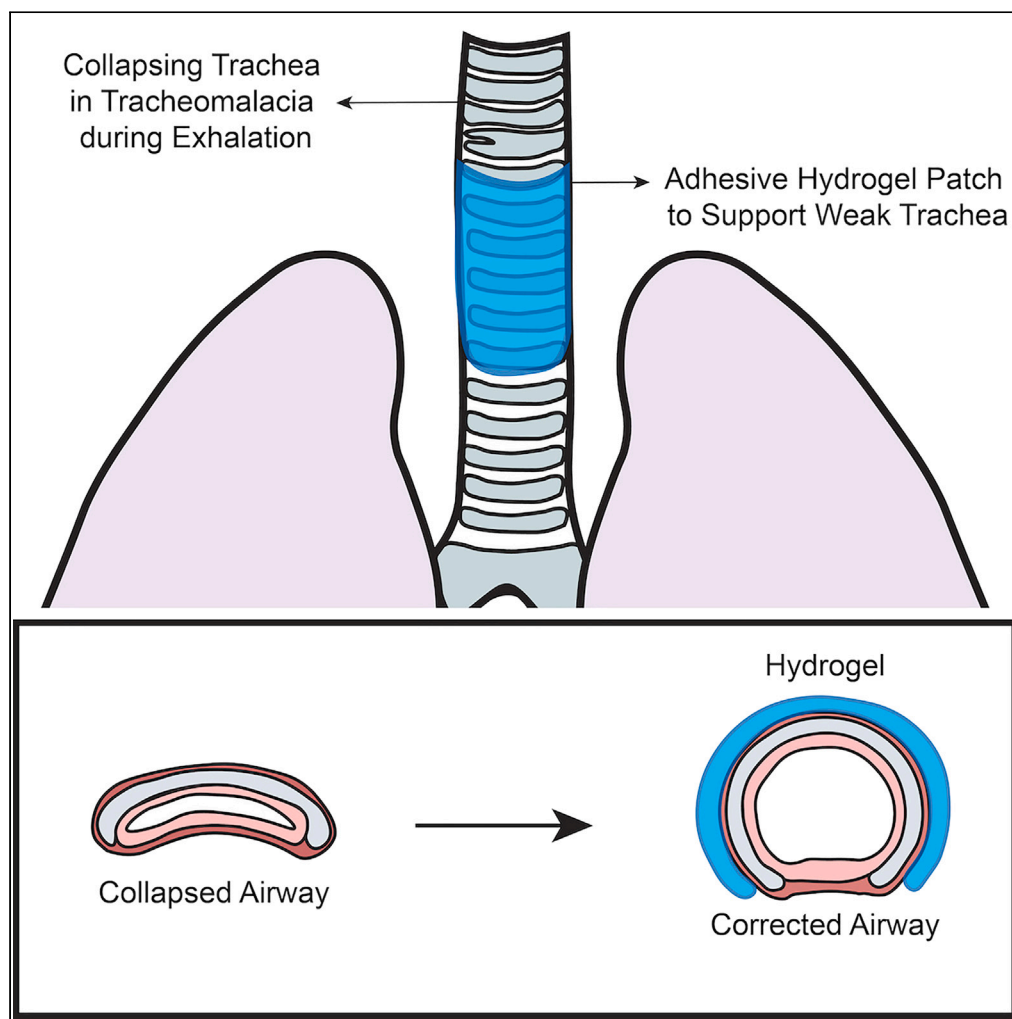**Article**

Wet adhesive hydrogels to correct malacic trachea (tracheomalacia) *A proof of concept*

Ece Uslu, Vijay Kumar Rana, Sokratis Anagnostopoulos, ..., Kishore Sandu, Nikolaos Stergiopulos, Dominique P. Pioletti

dominique.pioletti@epfl.ch

Highlights

Malacic trachea (Tracheomalacia) collapses and requires external mechanical support

Simulation indicated soft but adhesive hydrogel patch can hinder the airway collapse

HEAam-based adhesive hydrogels showed robust adhesion on tracheal surfaces

Adhesive hydrogels could be a promising approach to correct malacic trachea

Article

Wet adhesive hydrogels to correct malacic trachea (tracheomalacia) *A proof of concept*

Ece Uslu,[1,6] Vijay Kumar Rana,[1,6] Sokratis Anagnostopoulos,[2] Peyman Karami,[1] Alessandra Bergadano,[4] Cecile Courbon,[5] Francois Gorostidi,[3] Kishore Sandu,[3] Nikolaos Stergiopulos,[2] and Dominique P. Pioletti[1,7,*]

SUMMARY

Tracheomalacia (TM) is a condition characterized by a weak tracheal cartilage and/or muscle, resulting in excessive collapse of the airway in the newborns. Current treatments including tracheal reconstruction, tracheoplasty, endo- and extra-luminal stents have limitations. To address these limitations, this work proposes a new strategy by wrapping an adhesive hydrogel patch around a malacic trachea. Through a numerical model, first it was demonstrated that a hydrogel patch with sufficient mechanical and adhesion strength can preserve the trachea's physiological shape. Accordingly, a new hydrogel providing robust adhesion on wet tracheal surfaces was synthesized employing the hydroxyethyl acrylamide (HEAam) and polyethylene glycol methacrylate (PEGDMA) as main polymer network and crosslinker, respectively. *Ex vivo* experiments revealed that the adhesive hydrogel patches can restrain the collapsing of malacic trachea under negative pressure. This study may open the possibility of using an adhesive hydrogel as a new approach in the difficult clinical situation of tracheomalacia.

INTRODUCTION

Tracheomalacia (TM) is characterized by excessive luminal collapse because of immature cartilage formation and floppiness of trachealis muscle.[1] It can either be congenital or acquired. Congenital TM is the most common tracheal abnormality seen in neonates at an incidence rate of 1:2100.[2] Whereas an acquired TM can emerge because of infection, inflammation, tracheostomy, trauma, and compression exerted by abnormal cardiovascular structures.[2] Essentially a healthy trachea contains 18–22 anterior C-shaped cartilage rings as well as posterior membranous part. The trachealis muscle in the membranous trachea moves toward cartilage rings during exhalation and forceful efforts (crying, coughing, laughing, *etc.*) in intrathoracic segment of the trachea, which helps the airflow and mucus clearance.[2] During such movements, the openings of the airway lumen are narrowed down by 10–20% as depicted in Figure 1. Contrarily, if suffering from TM, the same cartilage rings tend to be U or bowed-shaped with broader and more dynamic trachealis muscles,[3] as portrayed in Figure 1. These changes in tracheal shape are accountable for airway collapse during expiration and forceful efforts in an intrathoracic segment of the trachea. This condition prevents normal breathing and could be life-threatening, especially for newborns.[1] In neonates, infants, and small children, tracheal lumen obstruction up to 50% because of a posterior to anterior collapse (tracheal muscle movement toward the cartilage ring) can be physiological, collapse exceeding 50% obstruction will cause respiratory symptoms and collapse >75% will be critical. Clinically, the collapse in the trachea can be classified as mild, moderate, and severe if it shrinks by 25–50%, 50–75%, and >75%, respectively.[4,5]

The main clinical approach to solve TM is to correct the geometry of the malacic trachea and to prevent the airway collapse. Depending on the severity, surgical interventions and stenting are commonly used treatment methods for TM. Surgical interventions like, aorto- and sterno-pexy alleviate the pressure by placing static suspension sutures on the trachea and attempt to increase the airway area.

However, these techniques are time-consuming and may fail if the pexy sutures breakdown. In addition, they are not indicated for TM cases requiring mechanical support as in a circumferential floppy airway, in form of external airway splints and endoluminal stents.[2,6–8] Alternatively, tracheal resection-anastomosis and slide tracheoplasty are used only for short segment TM which is seen seldom in clinics.[9] On the other hand, intraluminal stents (silicone, metallic and bioresorbable) and extraluminal splints (bioresorbable

[1]Laboratory of Biomechanical Orthopedics, Institute of Bioengineering, School of Engineering, EPFL, Lausanne, Switzerland

[2]Laboratory of Hemodynamics and Cardiovascular Technology, Institute of Bioengineering, School of Engineering, EPFL, Lausanne, Switzerland

[3]Department of Otorhinolaryngology, Airway Sector, University Hospital, CHUV, Lausanne, Switzerland
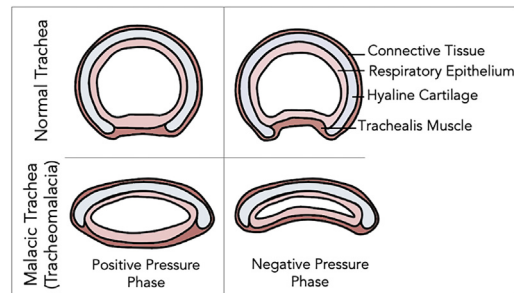
[4]Veterinary College, Bern, Switzerland

[5]Department of Anesthesiology, University Hospital, CHUV, Lausanne, Switzerland

[6]These authors contributed equally

[7]Lead contact

*Correspondence: dominique.pioletti@epfl.ch

https://doi.org/10.1016/j.isci.2023.107168

Figure 1. Representation of a normal and a malacic trachea during the positive and negative pressure phases of the respiratory cycle

plates and 3D-printed splints) have also been considered to correct the malacic trachea shape and stabilize the airway collapse by supporting the trachea mechanically.[10] However, both techniques come with numerous challenges to encounter. Intraluminal stents lead to severe complications in children, including stent obstruction because of secretions and granulation tissue, stent-induced stenosis, migration and erosion.[10] Extraluminal splints are fixed outside the tracheal lumen using sutures and have the advantages of avoiding complications of the endoluminal stent and support the structure externally.[11] However, the splint fixing piercing and sutures can cause obstructing granulations at the contact point inside the trachea and their rigidity could prevent the natural and dynamic neck movements in the child. Several reports indicate that the mechanics and materials design of the trachea should take into consideration longitudinal extension as an important factor. Physiologically, a healthy trachea may undergo longitudinal deformation of up to 20% in adults and up to 46% in babies.[12] Therefore, a rigid, solid tube design is unlikely to accommodate such a significant amount of deformation. In addition, this design would create a significant mechanical mismatch with the native tissue and further pulling on the fixation points may result in inflammation and fibrosis.[13] Fibrotic stenosis may also result from this, leading to increased airway resistance and abnormal respiration behavior, which can cause even the collapse of a mechanically suitable implant.[13] Furthermore, longitudinal tracheal deformation is a crucial factor for the epithelium, immune response, and secretion properties of the native tissue. It is well known that tracheal epithelium is highly sensitive to mechanical forces.[14–16] Tschumperlin and Drazen have shown that epithelial cells regulate the inflammatory response and fibroblast proliferation of the airway by generating related factors.[17] Therefore, a high stiffness material would create some problems related to inflammation-mediated fibrosis.

To understand TM condition broadly, we can look into a ubiquitous engineering problem in the piping industry. Pipes that are being used in the oil and gas industries often tumble if excess external pressure is applied.[18] The primary cause of pipe collapsing is inadequate mechanical properties of the materials utilized to manufacture them[19,20] and to prevent such unforeseen collapses, materials with better mechanical strengths could be paramount. Alternatively, depending on the severity of damage, an internal or external mechanical support to optimally support the pipe collapse could be a solution.

Inspired by the experiences developed in the pipe industry, here, we propose a proof of a new conceptual approach to correct TM where a malacic trachea can be supported mechanically by wrapping an adhesive hydrogel patch extraluminally. Hydrogels are 3D water-swollen polymers network that mimic the properties of many tissues.[21] These viscoelastic biocompatible materials allow the diffusion of oxygen, nutrients, and other molecules, which is an ideal environment for the cells to grow.[22,23] We envisioned that adhesive hydrogels could be employed to address numerous surgical challenges associated with treating TM. Adhesive hydrogels have the potential to eliminate the need for extraluminal stent fixation sutures, minimizing trauma to the surrounding tissues. In addition, the softness of hydrogels can provide the necessary flexibility to the trachea, reducing unnecessary pain during natural movement of the trachea in newborns when compared to stiffer materials.

Here, a numerical model was developed to test the hypothesis that external mechanical support provided by a hydrogel patch could prevent airway collapse. The model demonstrated that applying a hydrogel patch could help maintain a more natural shape of the trachea by restricting folding of the posterior tracheal membrane. Based on these findings, a new adhesive hydrogel was formulated using hydroxyethyl acrylamide (HEAam) and polyethylene glycol methacrylate (PEGDMA) as the primary polymer network and
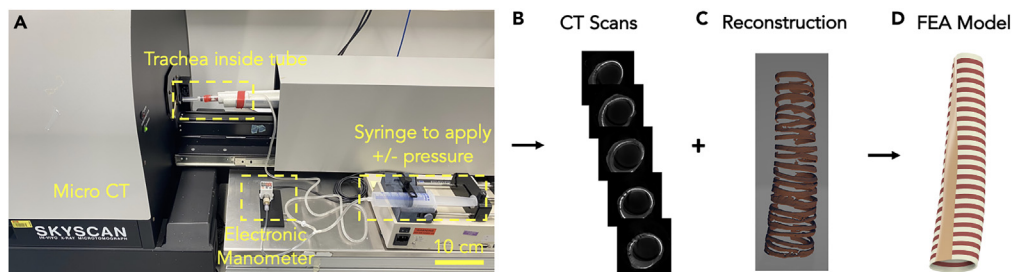
Figure 2. Experimental set-up and steps to obtain a simple trachea geometry for numerical model
(A) Micro-CT (μ-CT) machine, a set-up to fix the rabbit trachea inside the machine and to create the negative pressure using a syringe filled with air.
(B) Five equidistant cross-sections obtained from the μ-CT scanner.
(C) 3D reconstruction of the cartilage-to-tissue volume ratio.
(D) Generation of the final realistic model of equivalent geometrical properties.

crosslinker, respectively. These hydrogels provided strong adhesion to wet tracheal surfaces because of a two-step polymerization approach, which helped to anchor the surface more effectively and prevent collapsing. *Ex vivo* experiments were then conducted to assess the potential of this new approach in preventing collapsing in the tracheal membrane.

RESULTS AND DISCUSSION

A finite element analysis (FEA) model was developed to reinforce the hypothesis that local external mechanical support can hinder the airway collapse, and to understand the deformation and stress response of the trachea under maximum negative pressure with and without wrapping a hydrogel patch. The initial geometry was derived from μ-CT scans of the rabbit tracheas harvested in slaughterhouses. Subsequently, the 3D model was designed on AutoCAD Inventor, while all the numerical simulations were conducted on Ansys Mechanical. Thereupon, the trachea was placed inside the μ-CT machine, and a syringe-based vacuum system with an electronic manometer was connected to apply pressure (+/−) to deform it for later use, as shown in Figure 2A. To accurately capture the geometrical features of the trachea (the radially variable thickness, the asymmetric shape, etc.), five equidistant scans were used as a guideline to sketch the exact profile at the corresponding cross-sections (Figures 2B and 2C). A 3D model was then fitted through these sketches using a loft function, as shown in Figure 2D. Details are given in the STAR Methods section. Owing to their fibrous composition, it has been previously assumed in the literature that the tracheal components are incompressible, isotropic, and possess hyper-elastic properties.[24] The most accurate model for this type of materials is the Mooney-Rivlin model, which has been employed to represent the hyper-elastic properties of all three tracheal components (cartilage, muscle, and connective tissue).[25,26] Therefore, it has also been selected for this study. The strain-energy function generalized model can be defined as:

$$W = \sum_{i=1}^{2} a_i(I_i - 3)$$

where W is the strain energy, a_i are the constants of the material and I_i are the strain invariants. Additional information on the implementation of the Mooney-Rivlin model in Ansys can be found in the experimental and methods section.

To achieve mesh-independent results, a parametric study of multiple refined steps was conducted. The maximum deformation and von Mises stress converged after about $2 \cdot 10^5$ quad-dominant elements. The indicative results of deformation and von Mises stresses under −15 mmHg pressure are shown in Figures 3A–3D. The maximum deformation is experienced by the tracheal membrane, which is primarily responsible for the air blockage in the malacic tracheas. Expectedly, we noticed that the tracheal cartilage rings carry maximum stresses during tracheal deformation (or respiration).

We further simulated a trachea after wrapping a hydrogel patch to it under identical conditions. The hydrogel patch was modeled as a homogeneous material with Young's modulus (E) equal to 0.07 MPa, and a thickness of 0.7 mm (equal to the maximum thickness of the trachea ring). The membrane folding along
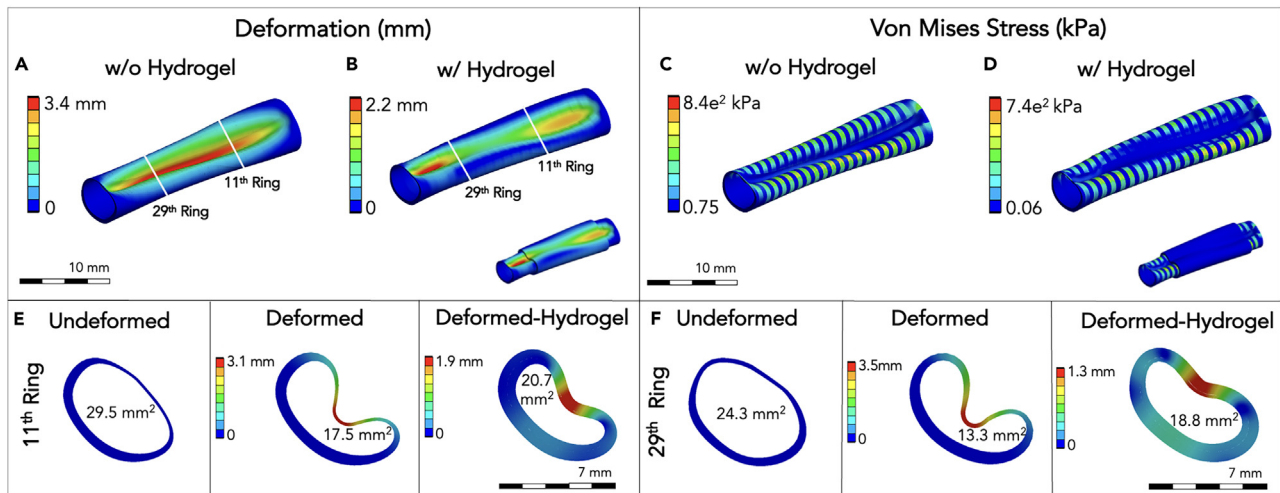
Figure 3. Indicative results of the total deformation and the stress distribution of a trachea at −15 mmHg
(A) Deformation of a trachea without hydrogel patch under applied pressure.
(B) Deformation of a trachea with hydrogel patch under applied pressure.
(C) Von Mises stress distribution of a trachea without hydrogel patch under applied pressure.
(D) Von Mises stress distribution of a trachea with hydrogel patch under applied pressure.
(E) Cross-sections of the rabbit trachea model at the 11th ring.
(F) Cross-sections of the rabbit trachea model at the 29th tracheal rings.

with the suction of the thinner cartilage endings have been captured by the large deformation model. As shown in Figures 3B and 3D, the deformation and stress values were reduced in a hydrogel-wrapped trachea. This strongly suggests that the hydrogel patch has the potential to constrain membrane folding. Specifically, the qualitative and quantitative results of the model show the deformation in the 11th and 29th tracheal rings under loading, as depicted in Figures 3E and 3F. The open area of the undeformed rings was 29.5 and 24.3 mm^2 and decreased to 17.5 and 13.3 mm^2 under −15 mmHg pressure, respectively. Of interest, the open airway area (degree of collapse) was improved by ∼11% and ∼23% once a hydrogel patch is applied to the 11th and 29th tracheal rings, respectively.

Based on the numerical findings, it is necessary for a hydrogel patch to be able to hold a trachea securely and prevent collapsing. This requires the hydrogel patch to have strong adhesive properties on the tracheal surface. Therefore, to identify the most suitable adhesive hydrogel that has the potential to prevent collapse, a series of adhesive hydrogels were synthesized by photo-polymerizing a mixture of hydroxyethyl acrylamide (HEAam) monomers and cross-linkers (Polyethylene glycol dimethacrylate (PEGDM) or Gelatin methacrylate (GelMA)) at specific ratios using lithium phenyl-2,4,6-trimethylbenzoylphosphinate (LAP) as a photoinitiator. The precursor solution was poured in a mold (15 × 15 × 0.7 mm^3) and illuminated under 405 nm light for 2 min to afford a covalently crosslinked 3D network of adhesive hydrogel patch, as shown in Figure 4A. A second polymerization was carried out after spreading the (same) precursor solution onto the trachea surface and a hydrogel film. A more detailed account of the synthesis and characterization of the adhesive hydrogels can be found in the STAR Methods section. To identify the most effective blend of HEAam and PEGDMA, we utilized wet rabbit trachea surfaces to screen different formulations and determine their shear adhesion strengths. We first varied the concentration of HEAam from 20 to 50 wt % while keeping the covalent cross-linking density constant (HEAam(%)/PEGDM(%) = 20), as shown in Figure 4B. Our results showed that increasing the monomer concentration to 40 wt % led to a 6-fold increase in shear adhesion strength from 10 kPa to more than 60 kPa. However, we did not observe any further improvement after this concentration. Therefore, we selected 40 wt % HEAam concentration to investigate the effect of PEGDM cross-linker (20kDa), as shown in Figure 4C. Our results showed that adhesion strength on trachea increased from 20 kPa to more than 60 kPa with increasing PEGDM concentration from 1 wt % to 2 wt %, respectively. However, at 3 wt % PEGDM concentration, we observed a decrease in adhesion because of higher cross-linking density of the gels, which led to brittleness and cohesive failures. Thus, we decided to choose 2 wt % PEGDMA concentration as the final crosslinker, in combination with 40 wt % of HEAam, to ensure a balance between adhesion and bulk properties of the hydrogel, which we named 40H-2Pgel.
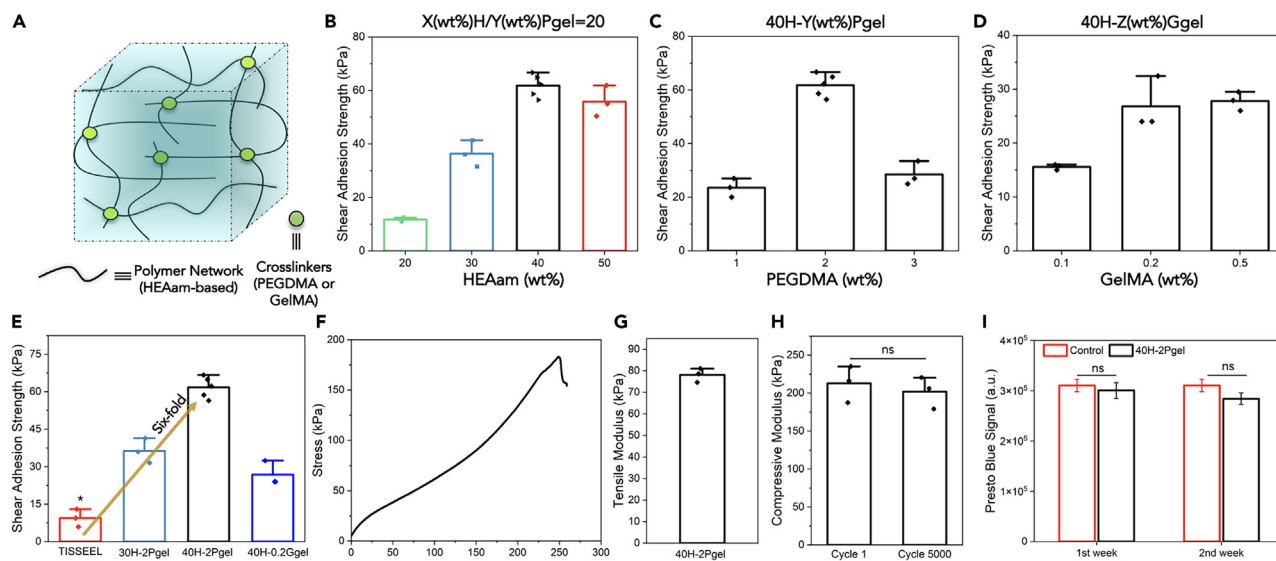
Figure 4. Characterization of the adhesive hydrogel

(A) Schematic of the adhesive hydrogel.

(B) Screening to find out the hydrogel formulation having highest shear adhesion strength on the wet rabbit trachea surface by changing HEAam concentration at fixed cross-linking density (HEAam(%)/PEGDM(%) = 20).

(C) Screening to find out the hydrogel formulation having highest shear adhesion strength on the wet rabbit trachea surface by changing PEGDMA concentration at constant HEAam concentration (40 wt %).

(D) Screening to find out the hydrogel formulation having highest shear adhesion strength on the wet rabbit trachea surface by changing concentration of another crosslinker GelMA at constant HEAam concentration (40 wt %).

(E) Shear adhesion strength of three hydrogels on the trachea and comparison with a commercial glue, TISSEEL.

(F) Typical stress-strain curve of 40H-2Pgel hydrogel.

(G) Tensile modulus of 40H-2Pgel hydrogel.

(H) Compressive modulus of 40H-2Pgel after cycle 1 and 5000.

(I) Cytotoxicity analysis of 40H-2Pgel after two weeks of incubation. *$p < 0.05$ compared to other samples. Data are represented as mean ± SEM.

We further explored the effects of GelMA as an alternative crosslinker, while maintaining a fixed concentration of 40 wt % HEAam (Figure 4D). Our research revealed that a lower concentration of GelMA (0.2 wt %) yielded the highest adhesion strength on the tracheal surface, which decreased significantly with the addition of more GelMA. Consequently, we selected 0.2 wt % GelMA and 40 wt % HEAam as the ingredients for our second hydrogel, which was named 40H-0.2Ggel.

We tested the shear adhesion strength of these hydrogel formulations in comparison to the commonly used surgical adhesive, TISSEEL, as demonstrated in Figure 4E. Our findings indicated that the 40H-2Pgel hydrogel had the highest shear strength of approximately 60 kPa on the wet tracheal surface (Video S1). This value was six times stronger than TISSEEL and approximately two times stronger than the 40H-0.2Ggel hydrogel.

The intrinsic adhesive properties of a hydrogel are because of the functional groups present on the polymer networks and their mechanical properties.[27–29] HEAam-based hydrogels (i.e., 40H-2Pgel) have two main functional groups -OH (hydroxyl) and -CONH- (amide) present on the polymer network.[30,31] These groups are crucial in forming multiple hydrogen bonds and strong van der Waals interactions with the tracheal surface, which has numerous functional entities, including primary amines (from lysine), carboxylic acids (from glutamic acid), thiols (from cysteine), and imidazole (from histidine).[32,33] When the polymer concentration is high, the hydrogel should interact more strongly with the tissue surface. This is why 40H-2Pgel showed higher adhesion on the tracheal surface than 30H-2Pgel. However, after reaching an optimum amount of polymer concentration (40 wt % HEAam), the physical interactions between the two surfaces saturate and reach a state where no further interactions can take place.

Covalent crosslinking is crucial in determining the bulk and dissipative (mechanical) properties of a hydrogel and is therefore important for achieving cohesive adhesion.[34,35] To achieve a robust and durable

adhesion, it is equally important to balance out the physical interaction (because of surface functional groups present on the polymer chains of hydrogel) as well as cohesive interaction between hydrogels and tissues.[32,36] However, a high crosslink density decreases polymer chain length and associated chain mobility, leading to the formation of a brittle hydrogel. This eventually reduces the hydrogel's adhesion strength.[37] Therefore, there was no observed adhesion improvement in hydrogel with high PEGDMA (>2wt %) concentrations. GelMA, on the other hand, is a non-linear bulky protein that can crosslink a hydrogel network at multiple sites (unlike PEGDMA). A high amount of GelMA led to a high crosslinking density, producing a brittle hydrogel,[38] and resulting in inferior cohesive properties for 40H-0.2Ggel. Therefore, 40H-2Pgel hydrogel was selected for further studies.

We examined the stress-strain curve and the modulus of 40H-2Pgel hydrogel under tension. The elastic modulus of hydrogel is ~75 kPa determined on the linear part of the stress-strain curve between 10 and 15% strain, as shown in Figures 4F and 4G. Because trachea is a dynamical organ, we also investigated the fatigue behavior of 40H-2Pgel hydrogel for up to 5000 cycle at 0.833 Hz to mimic the average breathing time in infants which is 1.2 s/breath.[13] As shown in Figure 4H, compressive modulus of the 40H-2Pgel showed no statistical difference after 5000 cycles, indicating the fatigue resistance of the gel under dynamic breathing conditions.

We then sought to investigate the cytotoxicity of the hydrogel. Viability tests of mouse embryonic fibroblast cells were performed up to two weeks. We found that after two-weeks of incubation, hydrogel did not exhibit any cytotoxicity and showing statistically no difference in PrestoBlue signal compared to a control, as shown in Figure 4I. This confirms the biocompatibility of 40H-2Pgel hydrogel, which is promising not only for TM but also for its potential use in other biomedical applications.

To confirm the numerical study and examine the potential of the developed adhesive hydrogel to prevent collapse, we scanned the malacic trachea obtained after the enzymatic degradation (see STAR Methods for the details) with and without the application of the adhesive hydrogel under −15 mmHg pressure in μ-CT and compared the experimental results with the numerical model. The enzymatic degradation should mimic a mild malacic condition in trachea after softening its cartilage rings. Figures 5A and 5B represents the synthesis and wrapping protocol of 40H-2Pgel hydrogel patch on a rabbit trachea for μ-CT measurements. To this end, a hydrogel splint (15 × 25 × 0.7 mm^3) was obtained and wrapped around a trachea by performing a two-steps photo-polymerization. The two open ends of a trachea lumen were airtight using stoppers and zip-closure, as shown in Figure 5B. Comparison between numerical and experimental results are shown in Figures 5C and 5D. It can be observed that the overall shapes of the cross-section areas agree well between the μ-CT scans and the numerical results (Figures 3E and 3F). The area of reconstructed and undeformed 11th and 29.5th tracheal rings was 29.5 and 24.3 mm^2, respectively, which is similar to the values obtained from the numerical model (29.1 mm^2 and 24 mm^2). Under the same negative pressure (deformed state), the cross-sectional area of these rings decreased to 19.5 and 15 mm^2, respectively. Likewise, the application of the adhesive hydrogel patch restrained the membrane movement and collapse by maintaining the airway area, specifically the inner area of the 11th (23.6 mm^2) and 29th (20.4 mm^2) rings is improved by 14% and 23%, respectively. These results validate the initial hypothesis and the numerical results. It is worth mentioning that even though the stiffness of 40H-2Pgel (~75 kPa, as shown in Figures 4F and 4G) is one order of magnitude lower than that of the trachea cartilage, the adhesive property of hydrogel is crucial to limit the suction of the muscle membrane in the tracheal lumen. These results provide assurance that biocompatible materials with adhesive properties and low stiffness can be effectively applied to the outer part of the tracheal membrane, resulting in a significant restriction of tracheal muscle deformation.

The 40H-2Pgel hydrogel was further tested in *ex vivo* studies with rabbit tracheas. At this stage, we considered creating extreme malacic conditions (>75% collapse[4]) by completely removing eight to ten cartilage rings from healthy tracheas (harvested from a government-notified slaughterhouse) by the surgeons at the Lausanne University Hospital CHUV, Switzerland, (Figures 6A and 6B). Subsequently, a negative pressure equivalent to the maximum physiological value (~5 kPa) was applied in a malacic trachea using a suction machine with an inbuilt manometer (Medela Surgicals, Switzerland) (Figure 6C), and airway collapsing behavior was recorded using a flexible bronchoscope (Exalt, 6mm, BUN20EXALTBSRT100, Boston Scientific), with and without wrapping a hydrogel patch (15 × 35 × 0.7 mm^3), as presented in Figures 6D, 6E, 6G and 6H. The images of a trachea from the outside indicate that the use of a hydrogel patch on a malacic trachea resulted in a significantly lower degree of collapse compared to the trachea without the patch and was comparable to the adjacent trachea (Figure 6H). It is important to note that each animal's trachea
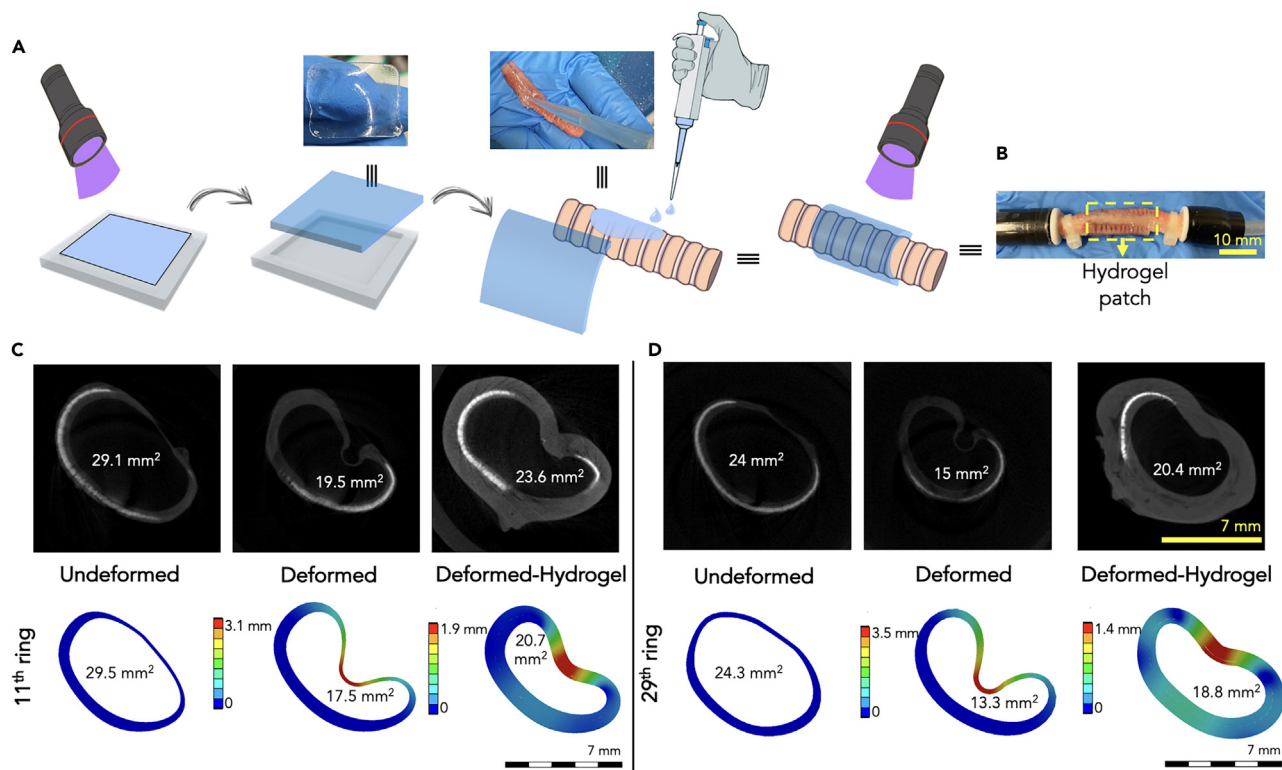
Figure 5. The potential of the adhesive hydrogel to prevent collapse in mild malacic conditions

(A) Schematic of a hydrogel-patch ($15 \times 25 \times 0.7$ mm^3) synthesis and preparation for a hydrogel-wrapped rabbit trachea, notably photo-polymerization was performed twice. For μ-CT analysis, rabbit trachea was kept in collagenase type 1 enzyme for 30 h to mimic mild TM conditions.

(B) A photo of a hydrogel patch-wrapped trachea where both openings were fixed using plastic clips to create negative pressure.

(C) μ-CT scans and numerical model of the 11th rings of trachea with and without application of the adhesive hydrogel at −15 mmHg.

(D) μ-CT scans and numerical model of the 29th rings of trachea with and without application of the adhesive hydrogel at −15 mmHg.

has different properties based on factors such as age, development, and severity of tracheomalacia. To maintain consistent results, we used a standardized process to create the hydrogel and chose a formula that was less susceptible to differences in trachea properties. For the hydrogel to be effective, it is crucial that it adheres well to the tracheal surface, preventing collapse and airway obstruction. Therefore, we used a bronchoscope during surgery to ensure the hydrogel adhered well and remained stable.

We further recorded the inner luminal movement by the bronchoscope and observed the behavior of a malacic trachea under a negative pressure, as shown in Figures 6F and 6I. Notably, without a hydrogel patch, airway was completely collapsed (Figure 6F, Videos S2 (outside) and S3 (inside)) whereas hydrogel wrapped malacic trachea shows up to 50% improvement in terms of airway opening (area = 82.5 mm^2) compared to the adjacent non-operated trachea (area = 170 mm^2, Figure 6I, Videos S4 (outside) and S5 (inside)). This strongly suggests that the collapsing of a malacic trachea can be mechanically corrected by wrapping an adhesive hydrogel patch extraluminally.

As a conclusion, tracheomalacia (TM) poses a life-threatening risk to newborns, and current treatment options have limitations that call for a better approach. To potentially reduce these shortcomings, we present the possibility of using an adhesive hydrogel patch that externally supports the malacic trachea to prevent airway collapse. Our numerical study demonstrated that the application of a hydrogel patch can preserve the physiological shape of the malacic trachea and constrain the membrane during collapse by holding it superficially. Building on our numerical findings, we formulated new adhesive hydrogels using hydroxyethyl acrylamide (HEAam) as the main polymer network and polyethylene glycol methacrylate (PEGMDA) as the crosslinker. Our biocompatible 40H-2Pgel hydrogel displayed a shear adhesion to the tracheal surface exceeding 60 kPa, a critical aspect of holding the trachea and preventing collapse. To test our approach, we wrapped the hydrogel patch around a malacic trachea and conducted micro-CT and *ex vivo*
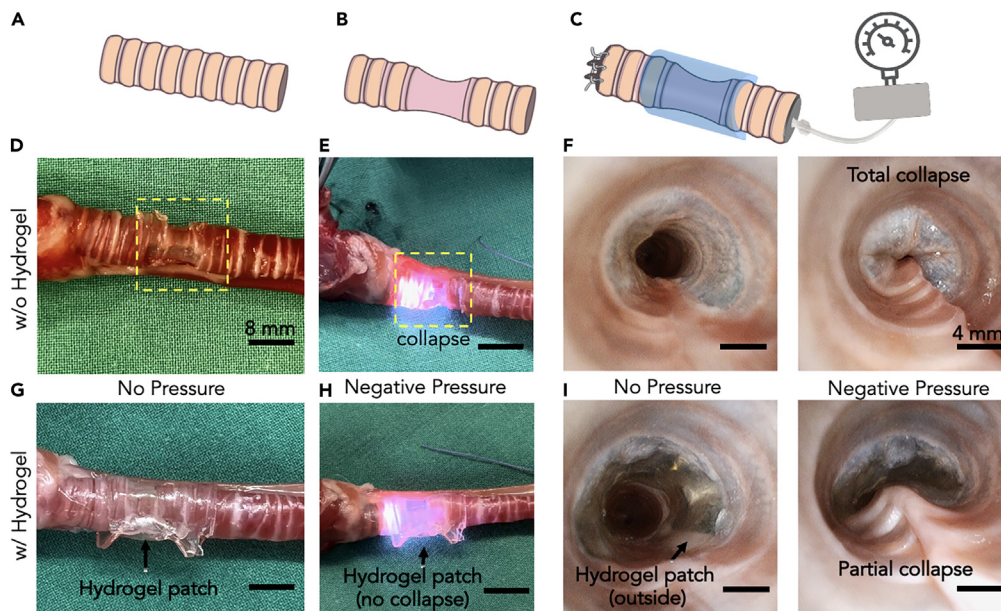
Figure 6. Procedure and results of *ex vivo* experiments

(A) Schematic of a normal trachea.

(B) Schematic of a malacic trachea (tracheomalacia).

(C) Flexible bronchoscope with an in-built suction channel with the hydrogel patch wrapping the malacic trachea. The distal end of the trachea was closed with surgical sutures to allow maximal negative pressure effect on applying the suction.

(D) An external view of a malacic trachea, cartilage rings were removed with preservation of the underlying mucosa to mimic tracheomalacia in a rabbit trachea.

(E) an external image of a malacic trachea under pressure that immediately collapsed even at a very low negative pressure (-1 to -2 kPa). The bright light is of the bronchoscope that visualized the tracheal lumen (see Video S2).

(F) Endoluminal image of the trachea under negative pressure captured by bronchoscope (see Video S3). Evidently, tracheal luminal structure was completely collapsed, a perfect example of the induced tracheomalacia.

(G) An external image of hydrogel patch ($15 \times 35 \times 0.7$ mm^3) wrapping the malacic trachea without any pressure.

(H) An external view of the hydrogel patch-wrapped malacic trachea with negative pressure. The bright light of the bronchoscope can be seen through the transparent tracheal mucosa. Airway collapse improved up to 50%, (see Video S4).

(I) Endoscopic luminal images further confirmed the improvement in collapse (see Video S5). Scale bars for external view of a malacic trachea and bronchoscope images with and without hydrogel are 8 and 4 mm, respectively.

measurements. Our results confirmed that the airway collapse was successfully hindered, highlighting the potential of our hydrogel patch as a promising solution for correcting TM.

Limitations of the study

While our study presents a promising approach to preventing collapse in TM using an adhesive hydrogel patch, there are several areas that require further investigation before progressing to *in vivo* studies for TM treatment. In particular, the adhesion strength of the hydrogel may be improved to prevent significant collapsing and enhance overall performance. As the trachea is in contact with body fluid, it is also important to ensure that the adhesive hydrogels do not show excessive swelling or degradation, which may impact their mechanical properties and adhesion.

STAR★METHODS

Detailed methods are provided in the online version of this paper and include the following:

- KEY RESOURCES TABLE
- RESOURCE AVAILABILITY
  - Lead contact
  - Materials availability
  - Data and code availability

- EXPERIMENTAL MODEL AND SUBJECT DETAILS
  - Cell lines
  - Animal organs
- METHOD DETAILS
  - Materials
  - Fabrication of adhesive hydrogel
  - Lap shear test
  - Numerical study
  - Micro (μ)-CT measurements
  - Tensile test
  - Fatigue test
  - Enzymatic degradation of tracheal cartilage
  - *Ex vivo* experiments
  - Toxicity test
- QUANTIFICATION AND STATISTICAL ANALYSIS

SUPPLEMENTAL INFORMATION

Supplemental information can be found online at https://doi.org/10.1016/j.isci.2023.107168.

AUTHOR CONTRIBUTIONS

Conceptualization: E.U., V.K.R., S.A., F.G., K.S., N.S., and D.P.P.; Methodology: E.U., V.K.R., and S.A.; Validation: E.U. and S.A.; Formal Analysis: E.U. and S.A.; Investigation: E.U. and S.A.; Writing – Original Draft: E.U. and V.K.R.; Writing – Review and Editing: E.U., V.K.R., S.A., P.K., A.B., C.C., F.G., K.S., N.S., and D.P.P.; Visualization: E.U. and V.K.R.; Supervision: V.K.R., F.G., K.S., N.S., and D.P.P.; Funding Acquisition: K.S., N.S., and D.P.P.

DECLARATION OF INTERESTS

The authors declare no competing interests.

INCLUSION AND DIVERSITY

We support inclusive, diverse and equitable conduct of research.

REFERENCES

1. Serrano-Casorran, C., Lopez-Minguez, S., Rodriguez-Zapater, S., Bonastre, C., Guirola, J.A., and De Gregorio, M.A. (2020). A new airway spiral stent designed to maintain airway architecture with an atraumatic removal after full epithelization—Research of feasibility and viability in canine patients with tracheomalacia. Pediatr. Pulmonol. *55*, 1757–1764. https://doi.org/10.1002/ppul.24816.

2. Kamran, A., and Jennings, R.W. (2019). Tracheomalacia and Tracheobronchomalacia in Pediatrics: An Overview of Evaluation, Medical Management, and Surgical Treatment. Front. Pediatr. *7*, 512–519. https://doi.org/10.3389/fped.2019.00512.

3. Choi, S., Lawlor, C., Rahbar, R., and Jennings, R. (2019). Diagnosis, Classification, and Management of Pediatric Tracheobronchomalacia: A Review. JAMA Otolaryngol. Head Neck Surg. *145*, 265–275. https://doi.org/10.1001/jamaoto.2018.3276.

4. Burg, G., Hossain, M.M., Wood, R., and Hysinger, E.B. (2021). Evaluation of agreement on presence and severity of tracheobronchomalacia by dynamic flexible bronchoscopy. Ann. Am. Thorac. Soc. *18*, 1749–1752. https://doi.org/10.1513/AnnalsATS.202009-1142RL.

5. Murgu, S.D., and Colt, H.G. (2006). Tracheobronchomalacia and Excessive Dynamic Airway Collapse. Respirology *11*, 388–406. https://doi.org/10.1111/j.1400-1843.2006.00862.x.

6. Hysinger, E.B. (2018). Laryngomalacia, Tracheomalacia and Bronchomalacia. Curr. Probl. Pediatr. Adolesc. Health Care *48*, 113–118. https://doi.org/10.1016/j.cppeds.2018.03.002.

7. Svetanoff, W., and Jennings, R. (2018). Updates on Surgical Repair of Tracheobronchomalacia. J. Lung Health Dis. *2*, 17–23. https://doi.org/10.29245/2689-999x/2017/1.1114.

8. Kamran, A., Smithers, C.J., Baird, C.W., and Jennings, R.W. (2021). Experience with bioresorbable splints for treatment of airway collapse in a pediatric population. JTCVS Tech. *8*, 160–169. https://doi.org/10.1016/j.xjtc.2021.04.010.

9. Wallis, C., Alexopoulou, E., Antón-Pacheco, J.L., Bhatt, J.M., Bush, A., Chang, A.B., Charatsi, A.M., Coleman, C., Depiazzi, J., Douros, K., et al. (2019). ERS statement on tracheomalacia and bronchomalacia in children. Eur. Respir. J. *54*, 1–19. https://doi.org/10.1183/13993003.00382-2019.

10. Gorostidi, F., Reinhard, A., Monnier, P., and Sandu, K. (2016). External bioresorbable airway rigidification to treat refractory localized tracheomalacia. Laryngoscope *126*, 2605–2610. https://doi.org/10.1002/lary.25918.

11. Gorostidi, F., Courbon, C., Burki, M., Reinhard, A., and Sandu, K. (2018). Extraluminal biodegradable splint to treat upper airway anterior malacia: A preclinical proof of principle. Laryngoscope *128*, E53–E58. https://doi.org/10.1002/lary.26857.

12. Harris, R.S. (1959). Tracheal extension in respiration. Thorax *14*, 201–210. https://doi.org/10.1136/thx.14.3.201.

13. Boazak, E.M., and Auguste, D.T. (2018). Trachea Mechanics for Tissue Engineering Design. ACS Biomater. Sci. Eng. *4*, 1272–1284. https://doi.org/10.1021/acsbiomaterials.7b00738.

14. Savla, U., Sporn, P.H., and Waters, C.M. (1997). Cyclic stretch of airway epithelium inhibits prostanoid synthesis. Am. J. Physiol. *273*, 1013–1019. https://doi.org/10.1152/ajplung.1997.273.5.L1013.

15. Gao, Y., and Vanhoutte, P.M. (1993). Responsiveness of the guinea pig trachea to stretch: Role of the epithelium and cyclooxygenase products. J. Appl. Physiol. *75*, 2112–2116. https://doi.org/10.1152/jappl.1993.75.5.2112.

16. Ressler, B., Lee, R.T., Randell, S.H., Drazen, J.M., and Kamm, R.D. (2000). Molecular responses of rat tracheal epithelial cells to transmembrane pressure. Am. J. Physiol. Lung Cell Mol. Physiol. *278*, 1264–1272. https://doi.org/10.1152/ajplung.2000.278.6.l1264.

17. Tschumperlin, D.J., and Drazen, J.M. (2001). Mechanical stimuli to airway remodeling. Am. J. Respir. Crit. Care Med. *164*, S90–S94. https://doi.org/10.1164/ajrccm.164.supplement_2.2106060.

18. Zhang, X., and Pan, G. (2020). Collapse of thick-walled subsea pipelines with imperfections subjected to external pressure. Ocean Eng. *213*, 107705–107714. https://doi.org/10.1016/j.oceaneng.2020.107705.

19. Christo Michael, T., Veerappan, A.R., and Shanmugam, S. (2012). Effect of ovality and variable wall thickness on collapse loads in pipe bends subjected to in-plane bending closing moment. Eng. Fract. Mech. *79*, 138–148. https://doi.org/10.1016/j.engfracmech.2011.10.009.

20. Ramasamy, R., and Tuan Ya, T.M.Y.S. (2014). Installation capacity assessment of damaged deepwater pipelines. MATEC Web Conf. *13*, 02003–02006. https://doi.org/10.1051/matecconf/20141302003.

21. Rafieian, S., Mirzadeh, H., Mahdavi, H., and Masoumi, M.E. (2019). A review on nanocomposite hydrogels and their biomedical applications. IEEE J. Sel. Top. Quant. Electron. *26*, 154–174. https://doi.org/10.1515/secm-2017-0161.

22. Chen, Q., Chen, H., Zhu, L., and Zheng, J. (2015). Fundamentals of double network hydrogels. J. Mater. Chem. B *3*, 3654–3676. https://doi.org/10.1039/c5tb00123d.

23. Rana, V.K., Tabet, A., Vigil, J.A., Balzer, C.J., Narkevicius, A., Finlay, J., Hallou, C., Rowitch, D.H., Bulstrode, H., and Scherman, O.A. (2019). Cucurbit[8]uril-Derived Graphene Hydrogels. ACS Macro Lett. *8*, 1629–1634. https://doi.org/10.1021/acsmacrolett.9b00717.

24. Bagnoli, P., Acocella, F., Di Giancamillo, M., Fumero, R., and Costantino, M.L. (2013). Finite element analysis of the mechanical behavior of preterm lamb tracheal bifurcation during total liquid ventilation. J. Biomech. *46*, 462–469. https://doi.org/10.1016/j.jbiomech.2012.10.036.

25. Martins, P.A.L.S., Natal Jorge, R.M., and Ferreira, A.J.M. (2006). A comparative study of several material models for prediction of hyperelastic properties: Application to silicone-rubber and soft tissues. Strain *42*, 135–147. https://doi.org/10.1111/j.1475-1305.2006.00257.x.

26. Safshekan, F., Tafazzoli-Shadpour, M., Abdouss, M., Shadmehr, M.B., and Ghorbani, F. (2020). Finite element simulation of human trachea: Normal vs. surgically treated and scaffold implanted cases. Int. J. Solid Struct. *190*, 35–46. https://doi.org/10.1016/j.ijsolstr.2019.10.021.

27. Karami, P., Nasrollahzadeh, N., Wyss, C., O'Sullivan, A., Broome, M., Procter, P., Bourban, P.E., Moser, C., and Pioletti, D.P. (2021). An Intrinsically-Adhesive Family of Injectable and Photo-Curable Hydrogels with Functional Physicochemical Performance for Regenerative Medicine. Macromol. Rapid Commun. *42*, e2000660. https://doi.org/10.1002/marc.202000660.

28. Li, J., Celiz, A.D., Yang, J., Yang, Q., Wamala, I., Whyte, W., Seo, B.R., Vasilyev, N.V., Vlassak, J.J., Suo, Z., and Mooney, D.J. (2017). Tough adhesives for diverse wet surfaces. Science *357*, 378–381. https://doi.org/10.1126/science.aah6362.

29. Yuk, H., Varela, C.E., Nabzdyk, C.S., Mao, X., Padera, R.F., Roche, E.T., and Zhao, X. (2019). Dry double-sided tape for adhesion of wet tissues and devices. Nature *575*, 169–174. https://doi.org/10.1038/s41586-019-1710-5.

30. Yu, X., Li, Y., Yang, J., Chen, F., Tang, Z., Zhu, L., Qin, G., Dai, Y., and Chen, Q. (2018). Nanoclay Reinforced Self-Cross-Linking Poly(N-Hydroxyethyl Acrylamide) Hydrogels with Integrated High Performances. Macromol. Mater. Eng. *303*, 1800295–1800311. https://doi.org/10.1002/mame.201800295.

31. Sun, X., He, S., Yao, M., Wu, X., Zhang, H., Yao, F., and Li, J. (2021). Fully-physically crosslinked silk fibroin/poly(hydroxyethyl acrylamide) hydrogel with high transparency and adhesive properties for wireless sensing and low-temperature strain sensing. J. Mater. Chem. C *9*, 1880–1887. https://doi.org/10.1039/d0tc05958g.

32. Nam, S., and Mooney, D. (2021). Polymeric Tissue Adhesives. Chem. Rev. *121*, 11336–11384. https://doi.org/10.1021/acs.chemrev.0c00798.

33. Muir, V.G., and Burdick, J.A. (2021). Chemically modified biopolymers for the formation of biomedical hydrogels. Chem. Rev. *121*, 10908–10949. https://doi.org/10.1021/acs.chemrev.0c00923.

34. Yi, M.B., Lee, T.H., Han, G.Y., Kim, H., Kim, H.J., Kim, Y., Ryou, H.S., and Jin, D.U. (2021). Movable Cross-linking in Adhesives: Superior Stretching and Adhesion Properties via a Supramolecular Sliding Effect. ACS Appl. Polym. Mater. *3*, 2678–2686. https://doi.org/10.1021/acsapm.1c00240.

35. Karami, P., Wyss, C.S., Khoushabi, A., Schmocker, A., Broome, M., Moser, C., Bourban, P.E., and Pioletti, D.P. (2018). Composite Double-Network Hydrogels to Improve Adhesion on Biological Surfaces. ACS Appl. Mater. Interfaces *10*, 38692–38699. https://doi.org/10.1021/acsami.8b10735.

36. Shen, J., Zhang, H., Zhu, J., Ma, Y., He, H., Zhu, F., Jia, L., and Zheng, Q. (2022). Simple Preparation of a Waterborne Polyurethane Crosslinked Hydrogel Adhesive With Satisfactory Mechanical Properties and Adhesion Properties. Front. Chem. *10*, 855352–855410. https://doi.org/10.3389/fchem.2022.855352.

37. Lee, J.H., Lee, T.H., Shim, K.S., Park, J.W., Kim, H.J., Kim, Y., and Jung, S. (2017). Effect of crosslinking density on adhesion performance and flexibility properties of acrylic pressure sensitive adhesives for flexible display applications. Int. J. Adhesion Adhes. *74*, 137–143. https://doi.org/10.1016/j.ijadhadh.2017.01.005.

38. Mathur, A., Li, A., and Maheshwari, V. (2021). Nanoscale Architecture of Polymer-Organolead Halide Perovskite Films and the Effect of Polymer Chain Mobility on Device Performance. J. Phys. Chem. Lett. *12*, 1481–1489. https://doi.org/10.1021/acs.jpclett.1c00004.

39. Zhu, M., Wang, Y., Ferracci, G., Zheng, J., Cho, N.J., and Lee, B.H. (2019). Gelatin methacryloyl and its hydrogels with an exceptional degree of controllability and batch-to-batch consistency. Sci. Rep. 9, 6863–6913. https://doi.org/10.1038/s41598-019-42186-x.

40. ASTM International, https://doi.org/10.1520/F2255-05R15 (accessed: April 2022).

41. Zweben, C., and Beaumont, P. (2017). Comprehensive Composite Materials II (Elsevier).

42. Safshekan, F., Tafazzoli-Shadpour, M., Abdouss, M., and Shadmehr, M.B. (2016). Mechanical Characterization and Constitutive Modeling of Human Trachea: Age and Gender Dependency. Materials (Basel) 9, 456–513. https://doi.org/10.3390/ma9060456.

STAR★METHODS

KEY RESOURCES TABLE

REAGENT or RESOURCE	SOURCE	IDENTIFIER
Biological samples		
Young Male Rabbit Tracheas (5-6 kg)	Delimpex AG, Pfäffikon, Switzerland	N/A
Chemicals, peptides, and recombinant proteins		
N-(2-Hydroxyethyl)-acrylamide (HEAam)	Chemie Brunschweig AG	Cat# H1262
Lithium-Phenyl-2,4,6 trimethylbenzoylphosphinat (LAP)	Sigma Aldrich	Cat# 900899
Polyethyleneglycoldimethacrylate (PEGDMA, M_n = 20kDa)	Polysciences	Cat#25406
Gelatin Type A from porcine skin	Sigma Aldrich	Cat#G2500
Methacrylic anhydride	Sigma Aldrich	Cat#276685
Sodium hydroxide	Sigma Aldrich	Cat#221465
Dialysis sacks (MWCO 6000– 8000 Da)	Spectrum Labs	Cat#132665T1
Hydrochloric acid	Sigma Aldrich	Cat#258148
Collagenase -I	Life Technologies	Cat#17100-017
Experimental models: Cell lines		
NiH/3T3 mouse embryonic fibroblast cells	ATCC	CRL-1658
Software and algorithms		
OriginPro 2021 Academic	OriginLab	https://www.originlab.com
ImageJ 1.51	National Institute of Health	https://imagej.nih.gov/ij/
AutoCAD Inventor	Autodesk	www.autodesk.com/products/inventor/overview
Ansys	Ansys, Inc.	ansys.com
Other		
Suction Machine	Medela Surgicals	N/A
Bronchoscope	Boston Scientific	N/A
E3000 linear testing machine	Instron	N/A
μ-CT machine	Skyscan	N/A

RESOURCE AVAILABILITY

Lead contact

Further information and requests for resources and reagents should be directed to and will be fulfilled by the Lead contact, Dominique Pioletti (dominique.pioletti@epfl.ch).

Materials availability

This study did not generate new unique reagents.

Data and code availability

- All data reported in this paper will be shared by the lead contact upon request.

- This paper does not report original code.

- Any additional information required to reanalyze the data reported in this paper is available from the lead contact upon request.

EXPERIMENTAL MODEL AND SUBJECT DETAILS

Cell lines

Fibroblast cells derived from mouse embryos (NiH/3T3, ATCC CRL-1658) were used to evaluate biocompatibility of the adhesive hydrogel under standard cell culture conditions (37°C and 5% CO_2 in humidified atmosphere) using complete cell culture medium (DMEM supplemented with 10% (v/v) Fetal Bovine Serum, 1% (v/v) Penicillin Streptomycin, 1% (v/v) L-Glutamine). Since cells were obtained from mouse embryos, there is no sex information available. Beside the information provided by the company, no further authentication tests have been done.

Animal organs

Male rabbit tracheas (weighing around 5-6 kg) were supplied by Meinrad Odermatt of Delimpex AG, Pfäffikon, Switzerland for experiments.

METHOD DETAILS

Materials

N-(2-Hydroxyethyl)-acrylamide (HEAam) was purchased from Chemie Brunschweig AG. Lithium-Phenyl-2,4,6 trimethylbenzoylphosphinat (LAP) was obtained from Sigma Aldrich. Polyethyleneglycoldimethacrylate (PEGDMA, M_n = 20kDa) was purchased from Polysciences. Gelatin Type A from porcine skin (ref. G2500), methacrylic anhydride, sodium hydroxide, and hydrochloric acid were purchased from Sigma Aldrich. Dialysis sacks (MWCO 6000– 8000 Da) were obtained from Spectrum Labs. Collagenase I was purchased from Life Technologies. Young rabbit tracheas (5-6 kg) were provided by Delimpex AG, Pfäffikon, Switzerland.

Fabrication of adhesive hydrogel

HEAam (20-50% w/v), PEGDMA (1 to 3% w/v), and photoinitiator LAP (0.05% w/v) were dissolved in PBS using vortex in absence of light. Gelatin methacrylate (GelMA) was synthesized following the protocol reported earlier[39] and used at concentration range of 0.1-0.5% w/v. In short, 10 wt % type B gelatin was dissolved in carbonate-bicarbonate buffer (0.25 M) at 55°C and pH of 9.4. Then, 0.938 mL of methacrylic anhydride was added to the solution and mixed well. Solution was kept at 55°C for 1 h. At the end of 1 h, pH of the solution was adjusted to 7.4 to finalize the reaction. Filtered solution were dialyzed against water at 50°C for 4 days. Finally, dialyzed solution was freeze-dried to obtain GelMA. The hydrogel precursor was poured into a 15x15x0.7 mm^3 custom-made Teflon molds and covered with plastic slides. Polymerization was achieved by the illumination of 405 nm light (3 mW cm^{-2}) for 2 minutes.

Lap shear test

Lap shear adhesion set-up based on ASTM F2255 standards[40] were used to measure shear adhesion of the hydrogels on a wet rabbit trachea surface. Rabbit tracheas were hydrated into PBS for 45 min before the adhesion measurements and cut into the dimension of 10x25 mm^2 (Figure S1A). Rabbit trachea piece was glued on the glass slide using Superglue (Loctite 401, Figure S1B). Once a hydrogel patch (15x15x0.7 mm^3) is prepared (as mentioned earlier), 100 μL of the precursor solution was poured onto wet trachea and hydrogel patch was placed on tissue surface avoiding any air bubble formation (Figure S1C). Furthermore, 100 μμL of the precursor solution was poured again on the top surface of the hydrogel patch and covered by glass slide (Figure S1D) followed by second photo-polymerization step for 2 minutes (Figure S1D). After second polymerization, adhesion measurements were performed using 50 N load cell connected to Instron E3000 mechanical testing machine with constant loading rate of 1 mm/s. Shear adhesion strength of the hydrogels was calculated dividing the maximum load by the surface area of the hydrogel patch. (n=3, where n represents the sample size.).

Numerical study

This section describes, step-by-step, the details of how numerical model was developed in this study.

Geometry

The geometry of the trachea was derived from one of the healthy rabbit tracheas (5-6 kg) that were scanned in the experimental study and was modelled on AutoCAD Inventor. In order to accurately capture the geometrical features of the trachea, like the radially variable thickness and the general asymmetric shape,

five equidistant scans were used as a guideline to sketch the exact profile at the corresponding cross-sections. A 3D model was then fitted through these sketches using a loft function. Subsequently, the 3D volume was divided in 44 regions (corresponding to 22 cartilage rings, 21 connective tissue and 1 muscle domains). To maintain the same ratio of cartilage-to-tissue volume, the partitioning process was based on an independent 3D reconstruction of the tracheal cartilage rings, which was produced on the open-source software Slicer.

Boundary and loading conditions

To facilitate the correlation between the experimental and the numerical results, the imposed boundary conditions on both ends of the trachea were chosen to be fixed. Thus, the longitudinal deformations were eliminated, but most importantly, any unwanted radial translations of the trachea which would be caused by the naturally present asymmetries, were minimized. Finally, the pressure load was applied on the internal surface of the geometry, facing the inward direction in order to describe the systolic behaviour during expiration. Based on the literature, the pressure experienced by the inner trachea walls during expiration is around -15 mmHg, hence it was the pressure of interest for the present numerical study.

Material properties

The Mooney-Rivlin model was selected for the present study as mentioned in the manuscript while the parameters inside Ansys were tuned according to the uniaxial stress-strain curves of a human trachea[26] and were assigned to the corresponding parts (Table S1). These parameters vary depending on the animal, age and gender[41] and could be further optimized for subject-specific measurements, but such a procedure lies beyond the scope of the present study.

Computational mesh

Through experimentation, the mesh strategy was proven to be an important factor for the stability but also for the convergence of the solution process. Several different strategies were attempted, including dynamic remeshing, and the most robust of which was to divide the geometry in the longitudinal domains of variable mesh density, according to their expected relative deformation, as shown in Figures S2A and S2B. Hexahedral elements were used where possible, due to their higher accuracy compared to tetrahedrons, while the quadratic element order was preferred to the linear, due to its ability to capture element bending.[42]

Deformation model

For the simulations, a static solver was selected since the main focus is aimed on the static behavior of the trachea under peak loading. However, the expected deformations are comparable to the radial direction (Figures S2A and S2B), which is the main direction of interest for malacic tracheas. This induces further geometrical non-linearities on the system, which require an iterative calculation of the stiffness matrix K at each pseudo-time step. For this reason, the large deflection model is selected in the software settings. It is worth mentioning that although using a linear model might converge to a rational solution, the internal strain energy of the material is not conserved. The comparison between a linear and a non-linear solution is shown in (Figures S3A and S3B), where it becomes apparent that a linear deformation model cannot accurately capture the shrinking of the trachea or the membrane folding (which were both observed in the experiments), while the non-linear model achieves both. For each sub-step of the solution, a direct solver is selected, as it has a positive impact on the computational time performance. The appropriate dynamic time-step for each pseudo-steady iteration is within the range of 10^{-5} and $4 \cdot 10^{-3}$ sec and it is chosen automatically by the solver.

Mesh independence

To achieve mesh-independent results, a parametric study of multiple refinement steps was conducted, where the average element size on each individual meshing domain was multiplied by a factor of $\sqrt[3]{1/2}$, in order to obtain a constant doubling of the total element number at each refinement. As shown in Figure S4A, both the maximum deformation and the maximum von Mises stress converges after about $2 \cdot 10^5$ elements. It can also be observed that the percentage of deformation improvement between the coarsest and the finest meshes is not higher than 2.5% (Figure S4B), which is an indication for the good quality of the mesh, as well as the suitability of the adopted domain division strategy. The runs were performed on a Ryzen 9 5900HX, while the timings for the coarsest and the finest runs were 3 min and 16 hours,

respectively. Thus, an intermediate model of $160 \cdot 10^3$ elements was selected which took around 6 hours to be solved. It should be mentioned that for parametric runs regarding the shape of the trachea, a coarser mesh could be used since the relative variation of the membrane deformation appears to be small (Figure S4B).

Micro (μ)-CT measurements

Two ends of the trachea were fixed to the stoppers and tightened with zip closure to make the trachea airtight. After that, healthy, malacic trachea and/or trachea with and without hydrogel patch ($15 \times 25 \times 0.7$ mm^3) were placed inside the μ-CT machine (Skyscan). The syringe was connected to the trachea to apply positive and negative pressure, and an electronic manometer was also connected to the plastic tubes to read the applied pressure values. Open area of the airway was calculated using ImageJ 1.51 software (National Institute of Health, Bethesda, Maryland).

Tensile test

The tensile tests of dog-bone shaped hydrogel specimens (2 mm thickness, 5 mm neck width and 4.5 mm gauge length) were carried out using an Instron E3000 linear testing machine (Norwood, MA, USA) with a 50 N load cell. The specimens were placed within the grippers and elongated at a loading rate of 0.1 mm. s^{-1}. The elastic modulus (tensile modulus) of the hydrogels was calculated on the initial linear slope of the tensile stress-strain curves at 10–15% strain (n = 4, where n represents n represents the sample size.).

Fatigue test

Cyclic compressive tests of the hydrogels (∅ 8.5mm) were carried out using an Instron E3000 linear testing machine (Norwood, MA, USA) with a 250 N load cell. Strain rate was calculated to mimic the average frequency of breathings in infants (1.2 s/breath). Samples were compressed up to 5000 cycles and 15% deformation. The compressive modulus of the samples was calculated between 5-10% strain using linear regression method (n=3, where n represents n represents the sample size). To prevent drying of the samples, portable humidifier was used during the fatigue experiment.

Enzymatic degradation of tracheal cartilage

To mimic the mild TM condition in a healthy rabbit trachea for μ-CT measurements, tracheal cartilages were degraded using 0.1% (w/v) collagenase-I (col-I) solution. Briefly, 500 μL of col-I solution was poured into a petri dish and fresh rabbit trachea was placed in it facing tracheal membrane upwards without interacting with col-I solution. To avoid dehydration, a custom-made water bath was used to float a petri dish (having trachea) on the water during degradation process. Degradation process was conducted for 12, 18, 24 and 48 hours. After each time interval, trachea was removed from the solution and washed thoroughly with PBS. Degraded (malacic) tracheas were stored at -20°C before further use.

Ex vivo experiments

To mimic the extreme TM condition, 8 to 10 cartilage rings were removed from a frozen and then thawed rabbit tracheas with scalpel without damaging the inner tracheal mucosa. The distal end of the trachea was closed using surgical sutures and ensure an air-tight condition. The flexible bronchoscope was introduced into the trachea through the laryngeal inlet. Hydrogel patch ($15 \times 35 \times 0.7$ mm^3) was prepared as described earlier. Then, precursor solution was poured on the trachea surface and wrapped with the hydrogel patch avoiding any air bubble followed by the second photo-polymerization using a portable torch for 2 minutes. Then, a negative pressure (-5 kPa, maximum physiological pressure) was applied to the trachea by suction set-up (Medela Surgicals) and collapse behavior was observed and recorded by a flexible bronchoscope (Boston Scientific). Experiment was repeated 3 times applying 20 +/- pressure cycles. Open area of the airway was calculated using ImageJ 1.51 software (National Institute of Health, Bethesda, Maryland).

Toxicity test

Fibroblast cells derived from mouse embryos (NiH/3T3, ATCC CRL-1658) were used to evaluate biocompatibility of the adhesive hydrogel. Briefly, the precursor of the adhesive hydrogel was filtered inside the laminar flow and poured into the sterilized disk-shaped molds (∅ 5mm). Then, molds were covered with glass slides and polymerization was performed for 2 minutes inside the laminar flow. After polymerization, the adhesive hydrogels were placed into 24-well plate filled with complete cell culture medium. Subsequently, the cell culture plate was placed into the incubator for 1 and 2 weeks. After fixed time intervals,

hydrogels were removed from the plate. The conditioned medium was put into 96 well-plates containing 1000 cells/well and incubated again for 1 day. After day one, medium was aspirated from the well-plate and 100 μL of 10% (v/v) PrestoBlue (A13261, Life Technologies) was put into each well and the plate was incubated for 30 min. After that, fluorescence was measured at 595 nm using a microplate reader (Wallac 1420 Victor2, PerkinElmer). Toxicity experiments were performed in triplicates using five replicates for each experiment. DMEM solution with 1000 cells/well was taken as control.

QUANTIFICATION AND STATISTICAL ANALYSIS

All data represented as mean $\pm$ SEM. Statistical parameters of the data were presented in the corresponding section of the methods above. The OriginLab software (Northampton, MA) and ImageJ 1.51 software (National Institute of Health, Bethesda, Maryland) were used for quantification. The OriginLab software (Northampton, MA) was used for statistical analysis of the data. One-way analysis of variance (ANOVA) with Tukey's test was applied for data analysis. $*p < 0.05$ was considered statistically significant.